WIND TUNNEL TESTS OF A WIND-POWERED CAR CARRIER

Erik Blackert KTH Royal Institute of Technology, Wallenius Marine, Sweden
Ulysse Dhomé KTH Royal Institute of Technology, Wallenius Marine, Sweden
Antonia Hillenbrand KTH Royal Institute of Technology, Oceanbird, Sweden
Carl Fagergren Wallenius Marine, Sweden
Jakob Kuttenkeuler KTH Royal Institute of Technology, Sweden
Frederik Gerhardt RISE, Sweden

To further improve the design and operation of modern sailing cargo vessels, additional knowledge of the interaction between multiple sails in combination with the hull is needed. This study investigates the aerodynamic performance of a fully sailing car carrier through an experimental test campaign with a large, fully instrumented model of the complete ship at the Volvo Cars Wind Tunnel in Gothenburg. The ship design is based on the latest version of the Orcelle vessel deigned by Wallenius Marine, which is a 217 m long car-carrier, equipped with six two element wingsails. The campaign focuses on evaluating multiple sail trims under varying apparent wind angles and different hull configurations. All tests are done at a chord based Reynolds number of approximately 0.9×10^6. *The evaluation involves measuring the aerodynamic forces through individual force measurements for each wingsail, combined with the overall force generated by the integrated hull and wingsail system, all measured in six degrees of freedom. The results highlight the importance of the sail trim and demonstrate how hull design influences wingsail performance. For apparent wind angles below 30°, reduced flap angles, a slender bridge, and trimming strategies that maximize forward thrust while minimizing yaw moment are favorable. At apparent wind angles closer to 90°, larger flap angles are preferred, bridge design becomes less critical, and maximizing forward thrust remains the primary trimming objective.*

1 Introduction

As of 2018, greenhouse gas (GHG) emissions from shipping accounted for approximately 2.9% of global emissions, a slight increase from 2.8% in 2012, indicating no trend toward reducing shipping's share of global emissions. In response, the International Maritime Organization (IMO) has set a target to reduce CO_2 emissions per transport work by at least 50% by 2050, in order to keep pace with global CO_2 reduction efforts.[1]

The obvious move to decarbonize the shipping sector is the adoption of carbon-neutral fuels. However, the existing global fleet as well as the lack of infrastructure for the production and handling of such fuels does not allow for an easy transition. Retrofitting current vessels is often not economically viable, as it typically requires a complete replacement of the onboard machinery and fuel supply systems. The cost of carbon-neutral fuels is expected to be higher than that of today's fuels. Additionally, investing in new ships, there remains considerable uncertainty about which fuel will emerge as the dominant energy source in the future. As a result, many new vessels are being designed with multi-fuel capabilities or are configured to allow easier retrofitting once the next generation of carbon-neutral fuels is established. This reflects the industry's cautious approach in the face of fuel market ambiguity, enabling individual shipowners to mitigate risk. [2]

As a result, wind propulsion has reemerged as a viable solution for reducing fuel consumption and emissions after completely disappearing from commercial shipping in the early 20th century. Wind-assisted propulsion, where conventional engines are complemented by wind propulsion technologies, allows vessels to maintain operational speeds while reducing fuel use no matter of which fuel the

vessel is operating on. As of January 2025 are approximately 50 vessels equipped with wind assisted propulsion, where most of them have been installed since 2020 and the order book is still increasing with a current amount of about 70 installations. [2][3]

To provide context for wind-assisted propulsion concepts, a brief review of relevant wind tunnel and CFD test campaigns is provided. During a wind tunnel test campaign investigating four rectangular hybrid wingsails on a bulk carrier, Fujiwara et al. [4] observed that the presence of the hull decreased the performance of the wingsails across all apparent wind angles (AWA), most notably under beam wind conditions. These tests were performed at a Reynolds number of 2×10^5. On average, the combined forward thrust of the four wingsails decreased from approximately 90% to 80% of the forward thrust of a single wingsail when comparing the configurations without and with the hull, respectively. Looking at the wingsails individually it was instead seen that the hull had a positive effect on the foremost wingsail for AWA up to around 70°. The presence of the hull reduces the forward thrust for all wingsails at AWA between 70° to 120°. Most of the negative influence of the hull was found to be mitigated by using a trimming strategy in which the angle of attack (AOA) gradually increases from the forward to the aft wingsails (Gradual Trim), instead of applying a parallel trim.

Wind tunnel experiments conducted by Bradbury et al. [5] investigate the performance of wingsail arrays on a vessel, examining variations in the number of wingsails and the AWA. These tests were performed at a Reynolds number of about 1×10^5. Arrays consisting of four, six, and eight wingsails were tested with parallel wingsail trim. The results show that as the AWA increases, the benefits of using a greater number of wingsails become more pronounced. At 90° inflow, the eight sail configuration not only generates the highest total thrust but also achieves greater thrust per wingsail compared to the four- and six-sail arrays. Only for the setup with eight wingsails are gradual trimming compared with parallel sail trim. The result shows that there are positive effects on lift when using other trimming strategies than parallel and specifically for AOA less than 90°.

The work of Bordogna et al. [6] investigates how the spacing between two rigid wingsails affects the force coefficients of the rig in a wind tunnel without the presence of a hull, tested at a Reynolds number of about 4.7×10^5. The wingsails where placed at a distance of 2.5 and 4 chord lengths between them. The wingsails were manually trimmed to maximize forward thrust. The forward thrust coefficient C_x generated by the two wingsails was compared to that of a standalone wingsail. The results show that the combined performance of the two wingsails exceeds that of the single wingsail for AWA between 35° and 165° for both wingsail spacings. The difference in forward thrust between the two spacings is minimal for all AWA but the larger wingsail spacing performs best at AWA between 90° and 120°. When analyzing the performance of each wingsail individually, it was found that the upwind wingsail consistently outperformed the downwind wingsail across all AWA up until 120°.

In Giovannetti et al. [7], the interaction between three tapered NACA 0015 wingsails was investigated in a wind tunnel without the presence of the hull. These tests were performed at a Reynolds number of about 6.7×10^5. Different trimming configurations were tested to determine the optimal trim. The results showed that for AWA up to 60°, the lift coefficient (C_L) of the forward most wing was higher than that of the standalone wingsail. The other two wings performed worse compared to a standalone wingsail for all AWA, except at 90°, where all three wingsails had equal C_L. The total C_x generated by the combined wingsails was highest at 90°.

In Reche et al. [8] 3D RANS simulations are used to systematically investigate the sail hull interaction of DynaRigs. The study shows that, when comparing three DynaRigs without hull interaction to those

with hull interaction, there is a performance increase between AWA 20° and 50°, with a maximum increase C_x of approximately 10% at AWA 30°. For larger AWA, there is instead a decrease of C_x, with the largest drop of about 20% occurring at 90° AWA.

The studies mentioned above show that the total C_X generated by a configuration consisting of multiple wingsails is highly sensitive to trimming, and that the presence of the hull significantly influences the results. Therefore, to accurately capture the performance of a sailing vessel, trimming must be investigated in combination with the hull. To this end, wind tunnel tests remain an effective method for testing complex model setups across a large test matrix.

This paper presents the results and key findings from the first wind tunnel campaign conducted at a Reynolds number of approximately 0.9×10^6, including six wingsails and a hull. To the authors' knowledge, tests of this scale and complexity have not previously been published. Comparable studies have been limited to Reynolds numbers between 1×10^5 and 2×10^5, a range in which airfoils exhibit abrupt changes in lift and drag characteristics [9]. The combination of high Reynolds number and an extensive test matrix makes the present campaign unique. Figure 1 shows the 5 m ship model equipped with six wingsails during the wind tunnel campaign.

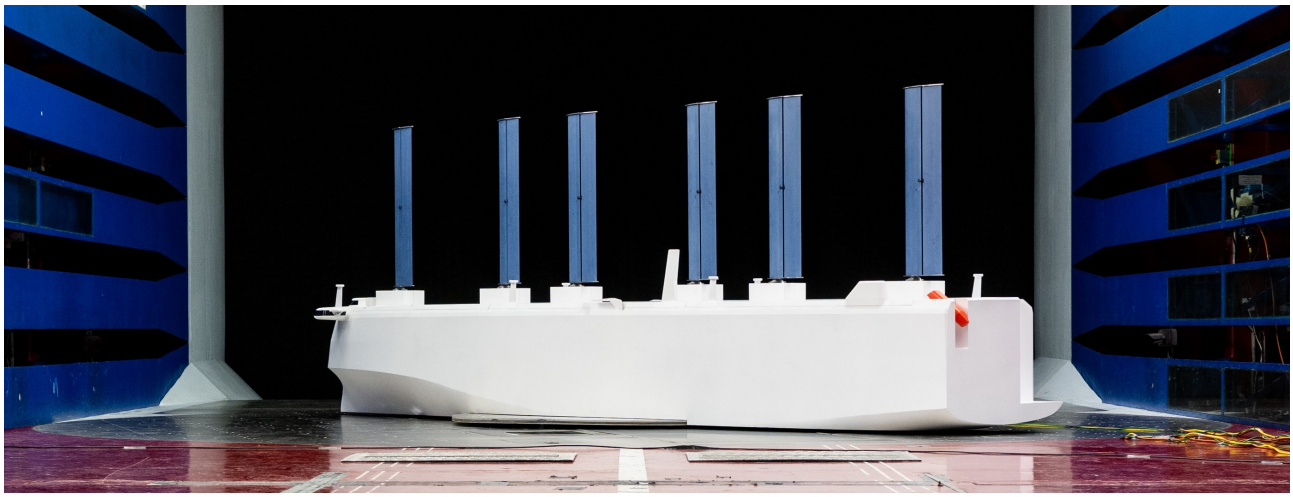

Figure 1: Picture of the tested ship model with 6 wingsails in Volvo's wind tunnel

The outline of the paper is as follows. Section 2 presents the test facility, model setup, and test program. The results and discussion of the wind tunnel test campaign are given in Section 3. Finally, the conclusions and future work are presented in Section 4.

2 Method

2.1 Test Facility

The wind tunnel used for this test campaign was the Volvo PVT Tunnel, a horizontally located closed-circuit wind tunnel. The test section has a length of 15.8 m, a width of 6.4 m, and a height of 4.1 m. The wind tunnel is equipped with slotted walls featuring an open area ratio of approximately 30%. The turbulence intensity at the turntable is about 0.1% in the x-, y-, and z-direction. According to [10], the boundary layer height at the center of the turntable is approximately 63 mm. The wind tunnel is equipped with a cooling system and the temperature is kept constant at 21° throughout the test campaign. The turntable is equipped with an underfloor balance that measures forces in six degrees of freedom (6-DOF) and allows yawing within a range of ±30°. The limitation of 60° rotation was solved

by attaching the model to a rotational plate on top of the turntable, thus raising the model by 20 mm above the floor. Although the tunnel can reach wind speeds of up to 70 m/s, a constant speed of 40 m/s was used throughout the entire campaign. This corresponds to a Reynolds number of approximately 0.9×10^6, based on the chord length of a wingsail with an undeflected flap.

2.2 Hull Design

The hull model used in these experiments is based on the *Orcelle Wind* design from Wallenius Marine, as of the end of 2024. The experimental model was built at a scale of 1:42, the main particulars are presented in Table 1. The vessel is equipped with six wingsails. The general layout of the hull and wingsails is illustrated in Figure 2. The wingsails are positioned along the centerline of the vessel at the following longitudinal distances from the Forward Perpendicular (FP): wingsail 1 at 21.2 m, 2 at 64.4 m, 3 at 86.0 m, 4 at 129.2 m, 5 at 150.8 m, and 6 at 193.0 m. To facilitate construction at model scale, detailed structural features of the hull and wingsails have been simplified.

Table 1: Main particulars of vessel

	Full Scale	Model Scale
Length Overall [m]	217	5.16
Breadth [m]	39.4	0.93
Height above waterline [m]	27.2	0.65
Capacity [CEU]	7300	-

The ship hull is constructed from high-density polymer and mounted on an aluminum frame that supports all measurement equipment. Inside the hull, six custom-designed force balances are installed to measure forces and moments accurately in 6-DOF. These balances are fixed in rotation; instead, each wingsail is free to rotate independently via the test control system, and its angular position is measured using a rotary encoder. The wingsails are actuated at a constant rotational speed of 0.5 degrees/second. The complete test assembly was designed and constructed by the maritime department of RISE, Research Institute of Sweden.

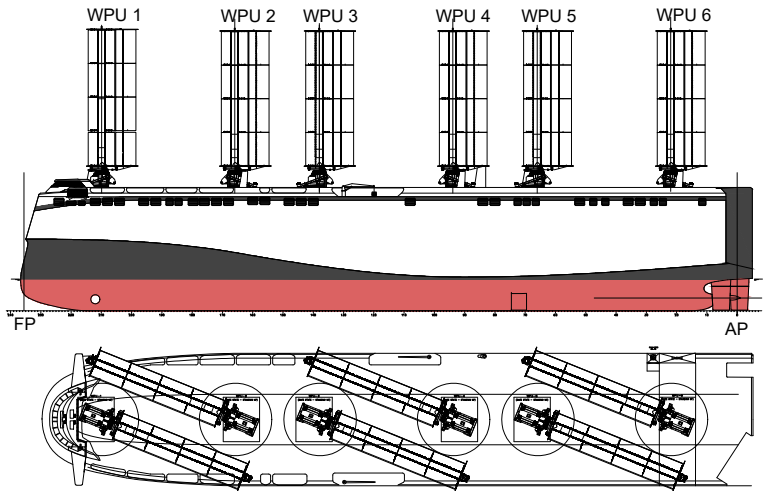

Figure 2: Schematic of the ship, top with raised wingsails in profile and bottom with tilted wingsails. seen from above. Forward Perpendicular is marked in the profile as FP.

2.3 Wingsail Design

The wingsail used in this experiment is a two-element wingsail designed by Oceanbird equipped with an actuated flap. The main element has a NACA 0025 profile, while the flap uses a NACA 0015

profile as seen in Figure 3. At full scale, the wingsail has a height of 40 m and a total chord length of about 14 m, giving a projected area with undeflected flap of 560 m^2. A more detailed description of the wingsail design is provided in [11]. For the purpose of this experiment, the wingsail was scaled down to 1:42, with certain simplifications made to facilitate model construction. The mast foot was replaced with a simplified square block, as replicating the steel structure and hydraulic actuation system accurately at this scale was considered unnecessary. The flap was fixed at a deflection angle of 20°, using the end plates for support, which removed the ability to adjust the flap angle during testing. Interchangeable endplates were used to change the flap angle to 0° and 10°. This was done to improve the stability and to simplify the construction of the model. The flap angle of 20° was chosen based on findings in [11]. No boundary layer tripping was applied to the wingsails. The surface was smoothed with K1000 sandpaper.

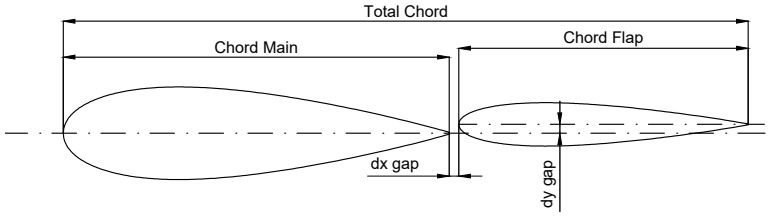

Figure 3: Schematic of the used two-element wingsail.

2.4 Coordinate system

All measurements are recorded in the ship's coordinate system, which is defined as right-handed: the x-axis points forward, the y-axis to starboard, and the z-axis downwards. The orientation of the coordinate system, wingsail and vessel is presented in Figure 4, showing a simplified version with only one wingsail.

The AWA is defined as the angle between the apparent wind direction and the vessel's centerline, positive for clockwise rotation of the apparent wind. The AOA is defined as the angle between the apparent wind and the chord line of the main profile, independent of the flap deflection angle, with positive values corresponding to a counterclockwise rotation of the wingsail in relation to the apparent wind. The flap deflection angle, DF, is defined as the angle between the chord line of the main element and that of the flap of the wingsail, with positive values corresponding to counterclockwise flap rotation.

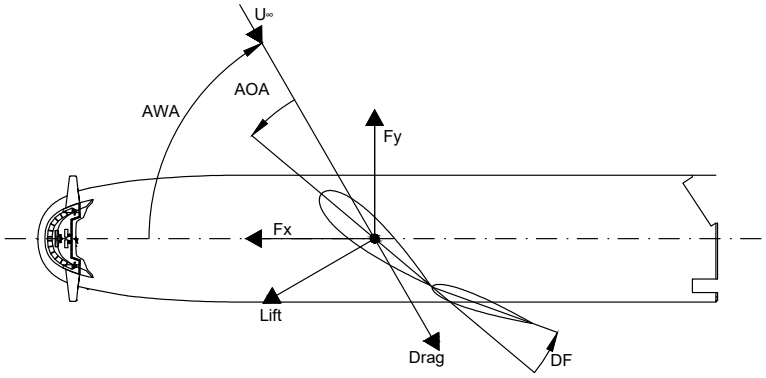

Figure 4: Schematic of the ship showing a single wingsail placed with its rotation axis on the centerline. All Angles in the graph are shown in their respectively positive direction.

2.5 Data acquisition

Throughout the entire test campaign, the following parameters were recorded: forces and moments in 6-DOF for each individual wingsail; the rotational angle of each wingsail; the combined forces and moments in 6-DOF for all six wingsails and the hull, measured by the wind tunnel's main balance, wind speed, air temperature, and AWA. For each test condition all measurements were sampled at a frequency of 100 Hz over a 20-second interval while the system was maintained at a fixed configuration. For each time series, the mean value was used to represent the measurement. In selected cases, the standard deviation was also computed to estimate oscillations in the wingsails, which may indicate near or stalled conditions [12]. To mitigate bias introduced by filters in the wind tunnel balance, the first 10 seconds of data were discarded when calculating the final average values.

2.6 Force Definition

The measured forces are presented in non-dimensional form, normalized according to Equation 1:

$$C_{i,j} = \frac{F_{i,j}}{\frac{\rho}{2} U_\infty^2 A_{\text{ref}}} \tag{1}$$

Here, i denotes the force direction in the ship's coordinate system x for thrust force and y for side force, and j indexes the individual wingsails or the total force of all wingsails and hull combined. A_{ref} is the projected area of a single wingsail measured as total chord times the span. When considering all six wingsails, the total force in direction i is given by $F_i = \sum_{j=1}^{6} F_{i,j}$, and the corresponding reference area becomes $A_{\text{ref}} = 6A_{\text{sail}}$.

For the combined contribution of the wingsails and the hull, the total force F_i is measured directly by the balance of the Volvo wind tunnel, and the reference area is $A_{\text{ref}} = \sum_{j=1}^{6} A_{\text{sail},j} + A_{\text{hull}}$, where A_{hull} represents the projected transverse area of the hull.

Lift C_L and drag C_D coefficients for the wingsails and hull forces are calculated from the thrust and side force coefficients using Equation 2 and 3, Where C_x and C_y could be that of an individual wingsail, all wingsails combined or total forces including wingsails and hull.

$$C_L = \sin(\text{AWA})C_x - \cos(\text{AWA})C_y \tag{2}$$

$$C_D = -\cos(\text{AWA})C_x - \sin(\text{AWA})C_y \tag{3}$$

The yaw moment for each wingsail is non-dimensionalized using Equation 4, where the yaw moment is positive in the clockwise direction when viewed from above. Consequently, a positive yaw moment turns the vessel towards the wind (decreasing AWA), while a negative yaw moment turns it away from the wind (increasing AWA).

$$C_{mz,j} = \frac{M_{z,j} + F_{y,j} L_{x,j}}{\frac{1}{2}\rho U_\infty^2 A_j L_{pp}} \tag{4}$$

Here, L_{pp} is the length between perpendiculars, and $L_{x,j}$is the longitudinal distance between wingsail j and the chosen yaw moment reference point. In this study, the yaw moment is calculated relative to the Forward Perpendicular (FP), as the hydrodynamic center of effort for this vessel type is typically located close to this point.

The vertical center of effort CE_z defined from the root of the wingsail, is calculated using Equation 5, where H_g is the height of the gap between root of wingsail and deck.

$$CE_{z,j} = \frac{\sqrt{M_{x,j}^2 + M_{y,j}^2}}{\sqrt{F_{x,j}^2 + F_{y,j}^2}} - H_{g,j} \tag{5}$$

2.7 Trimming Procedure

For each apparent wind angle, the sails were first manually trimmed to maximize the total driving force while maintaining a 4° margin to stall. These settings, hereafter referred to as the Baseline trim, were then used as the reference case for evaluating other trimming variations. The AOA of the individual wingsails for the baseline trim is presented in Figure 8f.

In total, seven trim variations around the baseline configuration were tested. These cases are summarized in Table 2. Variations (1) and (2) reduce the AOA, variation (3) increases the AOA, and variations (4)–(7) represent gradual trims with reduced AOA based on the wingsail location.

Table 2: All trimming variations around the baseline trim.

	Wingsail 1	Wingsail 2	wingsail 3	Wingsail 4	Wingsail 5	Wingsail 6
Var.1, -4° AOA	-4°	-4°	-4°	-4°	-4°	-4°
Var.2, -8° AOA	-8°	-8°	-8°	-8°	-8°	-8°
Var.3, +4° AOA	+4°	+4°	+4°	+4°	+4°	+4°
Var.4, 0 to -4° AOA	0°	-0.9°	-1.5°	-2.5°	-3.1°	-4°
Var.5, 0 to -8° AOA	0°	-1.9°	-3.1°	-4.9°	-6.1°	-8°
Var.6, -4° to 0 AOA	-4°	-3.1°	-2.5°	-1.5°	-0.9°	0°
Var.7, -8° to 0 AOA	-8°	-6.1°	-4.9°	-3.1°	-1.9°	0°

2.8 Test Matrix

The test campaign presented in this paper includes the main test matrix, foot-gap tests, flap angle tests, and evaluations of different bridge designs.

2.8.1 Main Test Matrix

The main test matrix includes all trim variations together with the baseline trim, evaluated at nine AWA 15°, 30°, 45°, 60°, 75°, 90°, 105°, 135°, and 160°, resulting in a total of 72 tests, all with flap angle of 20°.

2.8.2 Foot Gap Tests

To investigate the effect of removing the gap between the wingsails and the deck, the wings were designed with a removable mast foot extension. In the standard configuration, the gap was 0.114 m, and it was reduced to 0.004 m when the extension was removed.

Tests with minimal foot gap for all six wingsails were conducted at AWA of 15°, 60°, and 90°. The baseline trim and 20° flap angle was used for all cases in order to isolate the effect of removing the gap, totaling three tests.

2.8.3 Flap Angle Variations

The effect of different flap angles was investigated by testing two additional flap angles in addition to the standard 20° flap angle, two alternative settings 10° and 0° were tested. These flap angle tests were performed at AWA of 15°, 30°, and 60°. For each flap angle, the baseline trim configuration was tested. In addition, the wingsails were manually re-trimmed to identify improved values of C_x, specific to each flap angle, totaling nine tests.

2.8.4 Bridge Design Variation

The hull was designed with an interchangeable bridge structure to enable testing of two additional bridge configurations. The three bridge designs used during the test campaign are shown in Figure 5. Bridge A is the reference bridge, equipped with bridge wings, and was used as the default configuration for the remainder of the campaign. Bridge B is identical to Bridge A, except that the bridge wings are removed. Bridge C represents a more conventional, bluff bridge design commonly found on commercial vessels. Bridge B and Bridge C were tested at AWA 15°, 30°, and 60°, using the baseline trim and 20° flap angle in all cases.

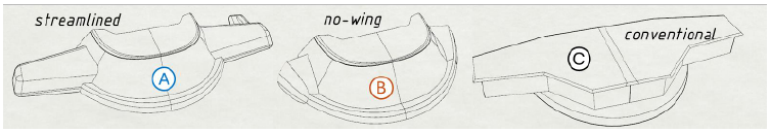

Figure 5: The three different bridge designs.

3 Results and Discussion

This section presents and discusses the results of the main test matrix, along with the effects of varying flap angles, the gap between wingsail and deck, and different bridge designs.

3.1 Wingsail performance for different trims

The force coefficients generated by the six wingsails with 20° flap angle, excluding the hull, are shown in Figure 6. Looking at C_x in Figure 6a the baseline trim performs best for AWA 30°, 45°, 60°, 75° and 135°. At AWA 15°, the differences in C_x between trims are minimal and difficult to distinguish during manual trimming. For AWA 90° and 105°, the +4° AOA trim performs best. C_x increases with increasing AWA and reaches its maximum at AWA 105°. A dip in the C_x curve is observed for AWA between 60° and 105° for all trims except the +4° AOA trim. This reduction in C_x was also reported by [4], where it was attributed to the presence of the hull. Since this dip is less pronounced for the +4° AOA trim, it remains unclear whether the effect is solely due to the hull or also influenced by improper trimming strategy of the wingsails. The influence of the hull is further examined in Section 3.5.

Figure 6b shows that C_y reaches its maximum for AWA between 30° and 45°. The difference in C_y between the different trim settings remains consistent for all AWA between 15° and 90°, with the highest C_x corresponding to the highest C_y, this agrees with the results shown in [7]. At AWA 15°, the differences in C_x between trims are minimal, but these are associated with relatively large differences in C_y, indicating that optimized trimming can drastically reduce the side force which has a positive effect on the leeway and the heeling of a vessel. As the AWA increases toward 90°, the difference in C_x becomes more significant, while the difference in C_y is constant, indicating that trimming for maximum C_x is preferred.

The fact that the highest values of C_x and C_L do not occur at the same trim setting across all AWA can be explained by the trade-off between lift and drag. For airfoils, an increase in C_L is accompanied by an increase in C_D due to the vortex generation associated with lift, commonly referred to as induced drag [13]. At low AWA, the x-component of C_L is small compared to the y-component, since $\sin(AWA) \ll \cos(AWA)$ for small AWA in Equation 2. For AWA close to 90°, however, $\cos(AWA) \ll \sin(AWA)$, and C_x therefore dominates C_L. Consequently, the trim setting that maximizes C_L does not necessarily maximize C_x, which explains why trims with the highest C_L do not correspond to the highest C_x for AWA up to approximately 30°.

The total lift and drag for the six wingsails are plotted in Figure 6c and 6d. The maximum C_L is reached at an AWA between 30° and 45°, which coincides with the highest C_D observed under upwind conditions. This maximum C_L for the six wingsails combined is 2.1. For comparison, [11] indicated that the maximum C_L of a single isolated wingsail with a 20° flap angle was about 2.0. This suggests that the efficiency of individual wingsails is increased due to the sail–sail interaction and the hull–sail interaction at AWA 45°. The highest C_D values occur at AWA 165°, where the drag has the largest positive impact on C_x due to the relation in Equation 2 and 3 as discussed in the section above.

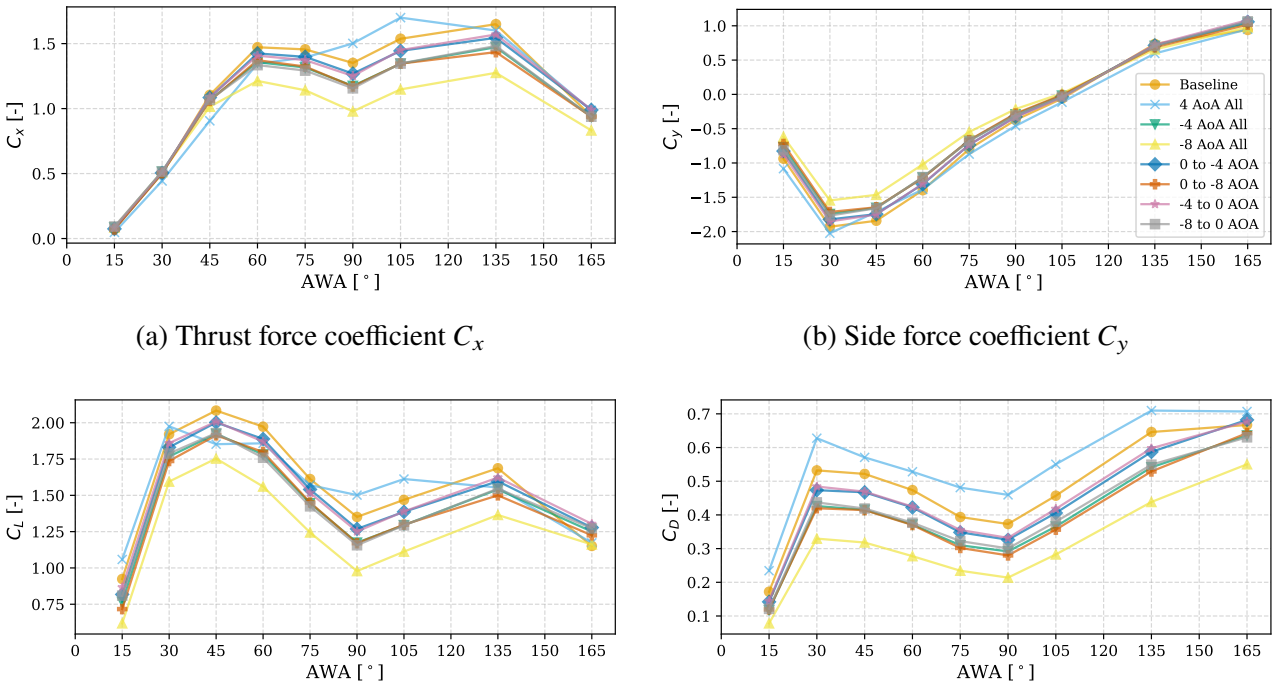

(a) Thrust force coefficient C_x

(b) Side force coefficient C_y

(c) Lift force coefficient C_L

(d) Drag force coefficient C_D

Figure 6: Force coefficients for the six wingsails for all tested trims with a flap angle of 20°

3.2 Relation between thrust and yaw moment

To analyze the relationship between C_x and c_{mz}, both coefficients are normalized with respect to the baseline trim. The results of this normalization are shown in Figure 7a for AWA 15°–75°, where C_x is plotted against c_{mz}; AWA 90°–165° are presented in Figure 7b. Due to the normalization, the baseline trim is positioned at $C_x = 1$ and $c_{mz} = 1$ for all AWA. It is important to note that c_{mz} is calculated around the FP of the vessel. Consequently, wingsails located further aft exert a larger influence on c_{mz}, further discussed in Section 3.5.

In Figure 7a, it can be seen that at an AWA of 15°, the three trims with the highest C_x values produce

nearly identical forward thrust, while their corresponding c_{mz} values differ by up to 30%. This indicates that c_{mz} can be reduced with almost no loss in C_x. At AWA 30°, the six points with the highest C_x values are nearly identical, yet their c_{mz} values differ by as much as 20%, again suggesting that yaw moments can be reduced without significant losses in forward thrust. For AWA between 45° and 75°, however, a trend is observed where a reduction in c_{mz} comes at the cost of decreased C_x. The same behavior is found for AWA between 90° and 165°, as shown in Figure 7b. These results demonstrate that proper trimming of the wingsails at AWA between 15° and 30° can substantially reduce the yaw moment without sacrificing forward thrust. At higher AWA, yaw moments can still be reduced, but only at the expense of reduced forward thrust. Assessing the impact of yaw moment on the vessel's forward speed would require a velocity prediction program, which is beyond the scope of this paper. In general, however, yaw moment leads to increased hydrodynamic resistance, as the rudder must counteract the yawing moment and thereby generating additional drag.

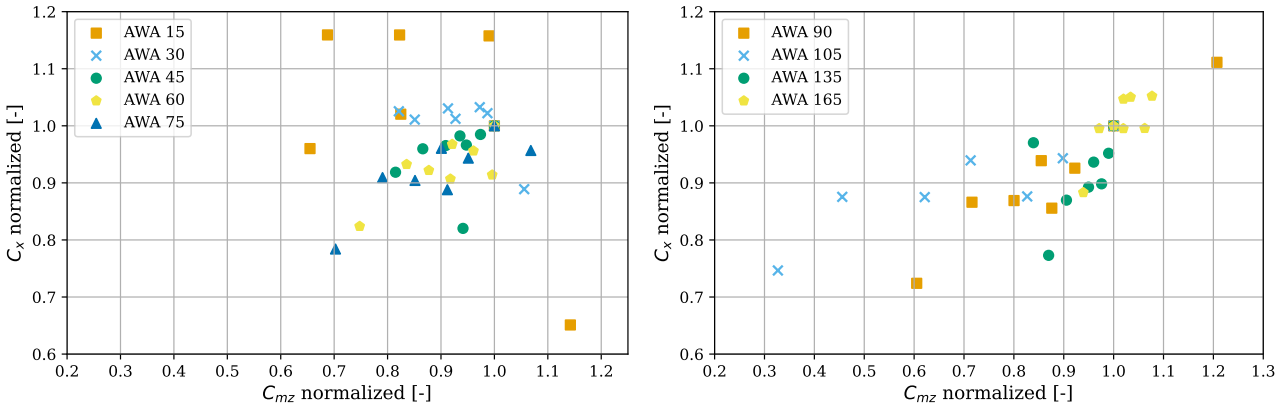

(a) Upwind conditions

(b) Beam reach and downwind conditions

Figure 7: Normalized C_x with baseline trim as reference plotted against normalized c_{mz}

3.3 Performance of individual wingsails

The forces and AOA of the individual wingsails for the baseline trim are presented in Figure 8. As shown in Figure 8a, C_x shows a clear trend up to an AWA of 60°, where wingsail 1 (the foremost wingsail) generates the highest thrust, and C_x decreases progressively with wingsail number. Additionally, wingsails appear to behave in performance pairs: wingsails 1–2, 3–4, and 5–6 show similar characteristics. Since the spacing between wingsails is not uniform, this pattern is likely influenced by their relative positioning. For AWA 105° and above, the pattern in which the forward wingsails have the highest C_x shifts; the aftmost wingsail, now closest to the wind, becomes the most effective wingsail. At AWA 165°, the relation between wingsail position and performance are less pronounced and no clear pattern can be seen.

At an AWA of 75°, there is a significant drop in C_x for wingsails–2 and 4 compared to wingsail 1 and 3 that maintain a higher C_x. Investigation of time series data of how the wingsail positioning for this trim was reached show no sharp drop of lift indicating stalling; however, the standard deviation in thrust for wingsail 2 and 4 is approximately 50% higher than for the other wingsails. This increased standard deviation may result from disturbed inflow caused by the hull and nearby wingsails, or it could indicate that these wingsails are operating near or beyond stall [12]. This behavior of reduced performance for wingsail 2 and 4 continues at AWA 90° and 105°, but no sign of stall is found here as well.

Figure 8b shows that, for AWA 15°, C_y is highest for wingsail 1, which is consistent with this wingsail

also exhibiting the highest C_x. At AWA 30°, the peak C_y is reached with wingsail 2. C_y for the individual wingsails are then reduced until reaching close to zero at AWA 90°. This shows once again that trimming to reduce C_y is most important at AWA between 15° and 60°.

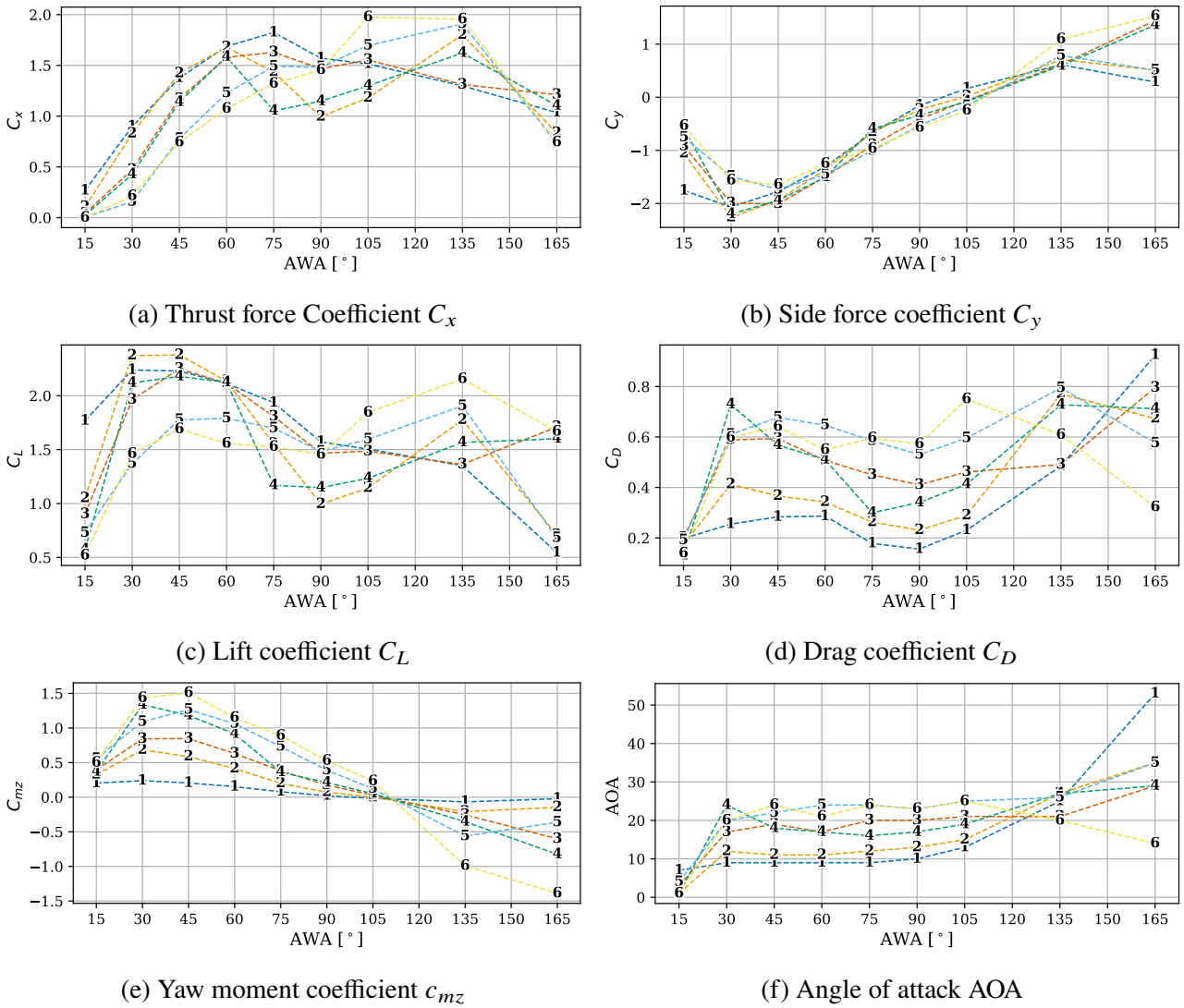

(a) Thrust force Coefficient C_x

(b) Side force coefficient C_y

(c) Lift coefficient C_L

(d) Drag coefficient C_D

(e) Yaw moment coefficient c_{mz}

(f) Angle of attack AOA

Figure 8: Coefficients for individual wingsails, including AOA, based on the baseline trim. The number on each line represents the wingsail number, with 1 being the foremost wingsail.

Figure 8c shows that at AWA 30° and 45°, the highest C_L among the individual wingsails is achieved by wingsail 2, reaching a value of 2.35. This is approximately 15% higher than that of an individual wingsail without hull influence [11]. The reason for this effect could be the positive impact between the wingsails or that the hull has a positive impact on the wingsails for these wind conditions. The influence of the hull could first be confirmed by repeating the experiments with the stand alone wingsails without the hull as in [4].

Figure 8d shows the drag coefficient C_D ranging from 0.1 up to 0.9. When compared to the data obtained for the individual wing in [11], this range is within that of the individual wingsail. The individual wingsail with a 20° flap angle stalls at a lift coefficient C_L of around 2.0 and then has a C_D of about 0.4. Based on the results in Figure 8c and 8d a correlation is shown between the loss of lift and the increase in drag coefficient for AWA 165° where it is more beneficial for C_x that the wingsails generate drag.

Since c_{mz} is calculated about the vessel's FP, wingsails positioned furthest aft have the greatest influence on the yaw moment. This relationship is clearly illustrated in Figure 8e. The yaw moment is positive up to an AWA of 105°, after which it becomes negative. The largest yaw moments occur at AWA 30–45° and 165°, with the highest values observed for wingsail 6. This highlights the importance of accounting for the yaw moment when trimming the aft sails. The effect is particularly pronounced at AWA 30–45°, where wingsail 6 shows the highest c_{mz} while simultaneously having the lowest C_x. In general, the six wingsails generate a yaw moment that turns the vessel into the wind for AWAs between 0° and 105°, and away from the wind for AWAs between 135° and 165°.

As seen in Figure 8f, the AOA of the individual wingsails increases the further aft they are located, with the exception of wingsail 4. This trend is valid for AWA between 30° and 105°. Exceptions to this trend are clearly observed at AWA 15°, 135°, and 165°. The observed AOA distribution does not fully match the gradual trim pattern suggested by [14] and [4], indicating that achieving optimal trim requires a methodology that accounts for the interaction between wingsails and for the specific hull shape. This allows for the inclusion of upwash, downwash and hull influence.

3.4 Flap angle influence on wingsail performance

The effect of varying the flap angle between 20°, 10°, and 0° is illustrated in Figure 9 for three different AWA. For flap angle 10° and 0°, the wingsails were manually retrimmed, and the best possible trim configuration was selected for evaluation. At AWA 15°, the highest C_x is achieved with a flap angle of 10°, resulting in a 35% improvement in C_x and a 14% reduction in c_{mz} compared to the 20° configuration. The 0° flap angle produces similar results. At AWA 30°, a flap angle of 10° improves C_x by 8% relative to 20°, while c_{mz} is reduced by 9%. The 0° flap angle leads to a 3% decrease in C_x compared to 20°, but significantly reduces c_{mz} by 30%. For AWA 60°, the 20° flap angle yields the highest C_x. However, the 10° and 0° configurations both result in a substantial reduction in yaw moment.

Overall, the results suggest that for low to moderate AWA (15°–30°), improved performance is achieved by reducing the flap angle. For AWA 60° a flap angle of 20° provides the best performance in terms of C_x. These findings are consistent with previous results presented by [5] where it was shown that the optimum camber increases with increasing AWA.

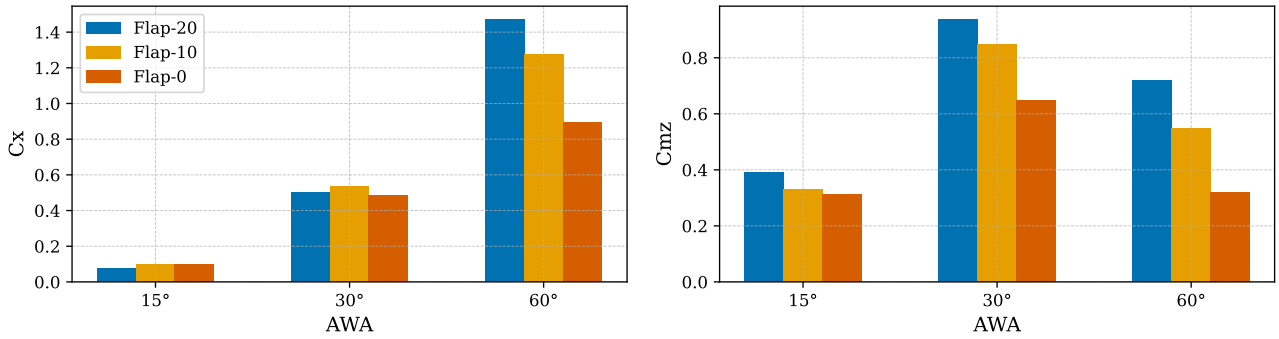

(a) C_x for different flap angles

(b) C_{mz} for different flap angles

Figure 9: C_x and C_{mz} for three different flap angles

3.5 Hull effect on wingsail performance

The effects of reducing the foot gap between the wingsail and the hull on C_L and Vertical Center of Effort CE_z are presented in Figure 10. For the case with a foot gap, CE_z is lowest at AWA 15° and 30°, with its location at about 47% of the span measured from the bottom of the wingsail. It then increases linearly up to AWA 90°, where it reaches a maximum of 56%. Beyond this point, CE_z decreases linearly to 53% at AWA 165°. The drastic decrease in C_L from AWA 45° to 90° coincides with the increase in CE_z. This indicates that part of the drop in C_L is due to the flow across the deck being more affected by the hull at AWA 90°, where the disturbed wind extends higher above the deck. Consequently, more force is exerted on the top of the wingsail relative to the bottom, leading to an increased CE_z.

Comparing CE_z and C_L when removing the foot gap of 0.114 m shows that at AWA 15°, the results remain almost unchanged. At AWA 60°, the location of CE_z increases from 50% to 55% of the span length, while C_L decreases by 0.2, corresponding to a 10% reduction. At AWA 90°, CE_z increases from 56% to 63% of the span, whereas C_L decreases by 0.23, corresponding to a 17% reduction. These results indicate that the positive effect of closing the foot gap, similar to placing an airfoil on a symmetry plane is outweighed by the negative influence of positioning the wingsail deeper into the disturbed wind.

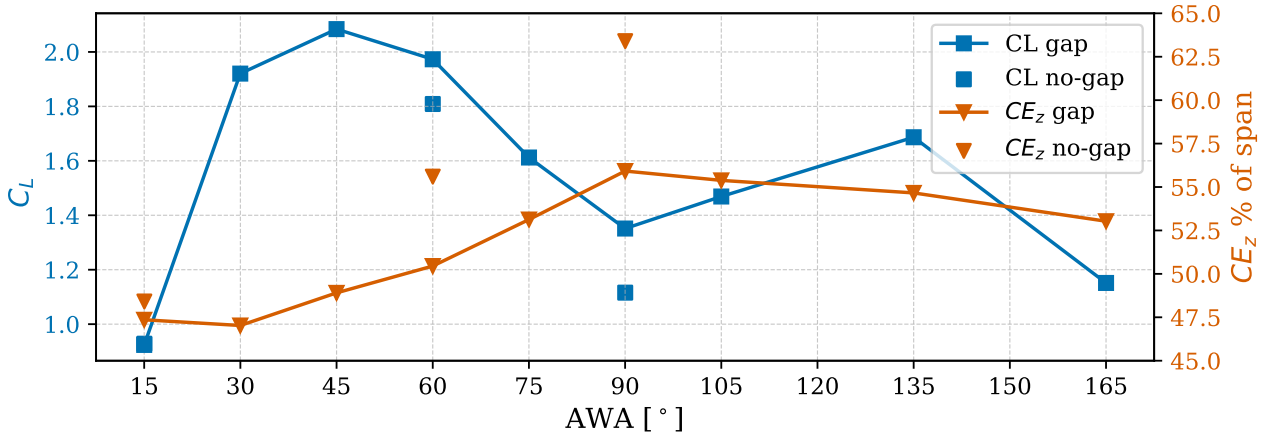

Figure 10: C_L and CE_z comparison between Gap and No-Gap wingsail arrangement, both arrangements have the baseline trim. CE_z is presented in % of the span length of the wingsail, measured from the root of the wingsail.

3.6 Bridge effect on wingsail performance

The effects of varying the bridge design between Bridge A, B, and C are shown in Figure 11. The absolute variations at AWA 15° are so small that they are excluded from this discussion, although they are shown in the figure. Figure 11a presents C_x for the six wingsails without the hull included. When only considering the wingsails, both Bridge B and Bridge C show a positive effect on C_x. Specifically, Bridge B improves C_x by 7% at AWA 30°, and minimal improvement in C_x at AWA 60°. For Bridge C, the improvement in C_x is 5% at AWA 30°, and minimal improvement in C_x for AWA 60°. When the total aerodynamic forces considering both wingsail and hull are evaluated as shown in (Figure 11b), the influence of bridge design changes. In this configuration, Bridge B increases C_x 13% for AWA 30° and no change in C_x for AWA 60°. In contrast, Bridge C results in identical C_x for AWA 30° and 60° compared to Bridge A. The result for total C_x, including the hull, shows that it is important to consider not only the wingsail forces when designing the bridge.

Overall, Bridge A and C perform almost identical with a small advantage to Bridge A. Bridge B consistently yields the highest C_x, making it the most favorable design, with a maximum C_x improvement of 12.7% at AWA 30°.

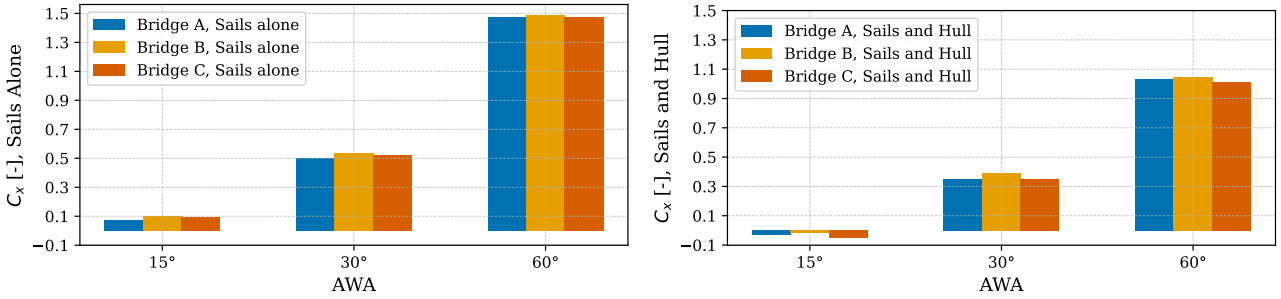

(a) C_x from wingsails alone

(b) C_x from wingsails and hull combined

Figure 11: C_x for three different bridge designs

4 Conclusion

This study investigated the aerodynamic performance of a six wingsail configuration together with the hull of a car carrier, tested in a wind tunnel under varying trim settings, flap angles, foot gaps, and bridge designs. The main findings can be summarized as follows:

- For different trim settings, the optimal configuration depends strongly on AWA. At 15°–30°, optimized trimming can reduce yaw moment by 20-30% without sacrificing forward thrust. A reduction in flap angle also has a positive effect at these AWA. For AWA closer to 90° the optimal trim can be focused on maximizing C_x without considering C_{mz} as much.
- The analysis of individual wingsails showed that the forward wingsails have the highest thrust coefficients up to 60°. The largest contribution to the yaw moment comes from the wingsail furthest away from the hydrodynamic center of effort. The AOA of the individual wingsails generally follows a pattern where the AOA increases progressively toward the aft.
- Removing the foot gap reduces C_L by 10% and 17% for AWA 60° and 90° respectively, demonstrating that the potential benefits of eliminating root-vortex effects are outweighed by increased exposure to disturbed flow above the deck.
- The bridge design has a minor impact. Where the streamlined bridge with bridge wings and the conventional bridge show almost identical performance, the bridge without bridge wings consistently yields the highest thrust, with a maximum improvement of 13% at 30°, making it the most favorable configuration. The improvements are however minimal at smaller and larger AWA.

Overall, the results highlight the importance of sail trim in combination with the interaction of the hull rather than in isolation.

References

[1] IMO, “Fourth IMO GHG Study 2020 Full Report,” tech. rep., London, UK: INTERNATIONAL MARITIME ORGANIZATION, 2021.

[2] DNV, "ENERGY-EFFICIENCY MEASURES AND TECHNOLOGIES - Key solutions and strategies for Maritime's decarbonization journey," tech. rep., DNV AS NO-1322 Høvik, Norway, 2025.

[3] Lloyds, "Applying wind-assisted propulsion to ships," research Report, Lloyds Register, Lloyd's Register, London, 2024.

[4] T. Fujiwara, G. E. Hearn, F. Kitamura, and M. Ueno, "Sail–sail and sail–hull interaction effects of hybrid-sail assisted bulk carrier," *Journal of Marine Science and Technology*, vol. 10, pp. 82–95, June 2005.

[5] W. M. S. Bradbury, "An Experimental investigation of the flow trough simplified multi-mast sailing rigs," tech. rep., Imperial College of Science and Technology, Department of Aeronautics, London,, London, Jan. 1984.

[6] G. Bordogna, J. Keuning, R. Huijsmans, and M. Belloli, "Wind-tunnel experiments on the aerodynamic interaction between two rigid sails used for wind-assisted propulsion," *International Shipbuilding Progress*, vol. 65, pp. 93–125, June 2018.

[7] L. M. Giovannetti, U. Dhome, K. Malmek, A. Persson, and C. Wielgosz, "Multi-Wing Sails Interaction Effects," in *SNAME 24th Chesapeake Sailing Yacht Symposium*, (Annapolis, Maryland, USA), p. D011S002R002, SNAME, June 2022.

[8] M. Reche Vilanova, S. Kaltenbach, P. Kourmoutsakos, H. B. Bingham, M. Fluck, D. Morris, and H. N. Psaraftis, "Predictive Surrogates for Aerodynamic Performance and Independent Sail Trim Optimization of Multiple Wind Propulsion System Configurations," *Journal of Sailing Technology*, vol. 10, pp. 19–49, Apr. 2025.

[9] S. F. Hoerner, *Fluid Dynamic Drag: Practical Information on Aerodynamic Drag and Hydrodynamic Resistance*. Brick Town, New Jersey, USA: Hoerner Fluid Dynamics, 1st ed ed., 1965.

[10] J. Sternéus, T. Walker, and T. Bender, "Upgrade of the Volvo Cars Aerodynamic Wind Tunnel," Apr. 2007.

[11] A. Hillenbrand, L. M. Giovannetti, U. Dhomé, and J. Kuttenkeuler, "Wind Tunnel Tests of a Two-Element Wingsail with Focus on Near-Stall Aerodynamics," *Journal of Sailing Technology*, vol. 9, pp. 110–127, Oct. 2024.

[12] S. Moreau, M. Roger, and J. Christophe, "Flow Features and Self-Noise of Airfoils Near Stall or in Stall," in *15th AIAA/CEAS Aeroacoustics Conference (30th AIAA Aeroacoustics Conference)*, (Miami, Florida), American Institute of Aeronautics and Astronautics, May 2009.

[13] J. Eastman, "No. 460 The characteristics of 78 related airfoil sections from tests in the variable density wind tunnel," Technical Report NACA Technical Report No. 460, National Advisory Committee for Aeronautics, Washington, D.C., Jan. 1935.

[14] W. M. S. Bradbury, "An Investigation of Graduated Trim for an Aerofoil Rig," (London), Royal Institution of Naval Architects, 1980.